

Using complex networks to model 2-D and 3-D soil porous architecture

Sacha Jon Mooney¹ and Dean Korošak^{2,3}

¹*Environmental Sciences Section, School of Biosciences, University of Nottingham,
University Park, Nottingham NG7 2RD, U.K.*

²*Center for Applied Mathematics and Theoretical Physics, University of Maribor
Krekova 2, Maribor SI-2000, Slovenia*

³*University of Maribor, Faculty of Civil Engineering, Chair for Applied Physics
Smetanova ulica 17, Maribor SI-2000, Slovenia*

Abstract

The ability to quantify three dimensional (3-D) soil porous architecture is a key requirement in the advanced understanding of soil functioning. Recent developments in the visualisation of soil structure using tools such as X-ray Computed Tomography (CT) provide new opportunities for enhancing the predicating capacity of new and established methods for pore scale modelling. Here we apply a novel complex networks approach in an attempt to unfold the complexity of soil pore architecture in both two and three dimensions. Using images of soil structure obtained by X-ray CT, we constructed and successfully validated a complex network derived from a simple measure of soil pore connectivity in two dimensions (2-D). We were able to illustrate that the examined soil comprised a scale-free network that could be adequately characterised by a power-law degree distribution. This was supported by random walk simulations performed on the soil images which demonstrated sub-diffusive behaviour. The soil pore structures exhibited larger correlations values for short distances compared to randomly generated images and slower decay of correlations. Finally, we derived an algorithm to generate a modelled soil structure built on the underlying scale-free network which was in close agreement with an actual 3-D reconstructed soil structure even though it was computed without any pore specific reference to the real soil sample besides the volume of the sample and the porosity. Considering the soil system as a complex network with scale-free properties is likely to have important consequences for the further understanding of transport in soils.

Keywords: complex networks, X-ray Computed Tomography, soil structure, porosity, pore connectivity.

Introduction

Description and subsequent quantification of soil pore structure is important to promote our understanding of soil function as pore spaces are the environment for all biological, chemical and physical processes within the soil. The structure of soil is the 3-D dynamic, heterogeneous framework in and through which all soil processes occur (Young & Crawford, 2004). Whilst it is recognised the pore morphology of soil has a profound effect on soil function, most existing theories for these functions do not adequately account for pore geometry and, as such, cannot be used for the development of fully mechanistic models (Cislerova, 1999). As a direct result, there is a need to develop an understanding of how porous structure affects the specific function of soils. However, despite considerable advances in recent years, knowledge is fragmented because traditional methods of structural measurement are either destructive or based on observations solely in 2-D. This is a severe limitation for spatio-temporal examination of 3-D soil pore structure and associated soil functions (Vogel, 1997). However, recent advances in non-destructive imaging, such as X-ray CT, provide new opportunities to examine the soil physical environment.

Pore network models are generally based on attempts to idealise pore tomography into a hydraulically similar but much simpler geometry in a regular network. The earlier network models used spheres and cylindrical throats (see Lin et al., 1999). Modern pore network models allow irregular throats so that more-than-one fluid phases can share a single pore, which is more realistic (e.g. Vogel et al., 2005). However, some issues still remain unresolved such as how to correctly represent the spatially correlated pore geometry existing in natural porous media when constructing predictive network models. Today numerous approaches to describing and modelling the complex geometry of soils exist including fractal theory, Boolean random sets, cellular automata and network models. (Bird et al., 2006; Horgan and

Ball, 1994; Prosperini and Perugini, 2007; Vogel and Roth, 2001). Recently Blair et al. (2007) have shown that 3-D neighbourhood probability models derived from 2-D thin sections can be developed that show good agreement with soil metrics from high porosity soils but are less successful in lower porosity soils (<11%) which could apply to many soil types.

In network models, the quantification of the topology of pore networks is usually based on the cubic, fixed grid lattice (Vogel and Roth, 2001) with defined a connectivity function (Vogel, 1997). The topology of pore space can be quantified by the connectivity given by the number of independent paths between two points (Spanne et al., 1994). Very recently it was demonstrated fractures in rocks can be modelled as a 'small-world' network (Valentini et al., 2007). This small-world network is an example of a complex network showing short average path between vertices and high local connectivity. However, to date no small world complex network approaches for understanding soil pore structure have been developed.

Complex network theory has recently attracted large attention across several scientific disciplines as it can be used to describe very diverse systems from the network perspective (e.g. Albert and Barabasi, 2002; Newman, 2003). We hypothesise the complex network approach could lead to significant new insights into soil pore geometry especially considering recent studies of self-similarity (Song et al., 2005) and self-organization (Kim et al., 2005) of complex networks.

Here we present a new approach towards unfolding the complexity of soil pore architecture utilising complex network theory. Using a series of 2-D images of undisturbed soil structure derived by X-ray CT, our approach is based on a combination of network and random set models (Horgan and Ball, 1994) where we first measure pore connectivity and subsequently

construct the complex network of pore architecture. From this we will develop a 2-D soil structural model from a simple set of rules based on a complex network approach which is correlated with the original soil structural image. Finally we will compute a 3-D model using the same complex network approach and compare with a 3-D representation of soil porous architecture reconstructed from a stack of CT 2-D images.

Materials and Methods

Undisturbed soil samples (170 mm length x 170 mm diameter) were obtained from the University of Nottingham's experimental farm at Sutton Bonnington from the Dunnington Heath series, a sandy loam (Stagno Gleyic Luvisol). The samples were scanned using a Phillips Mx8000 IDT 16 series whole body X-ray CT scanner. The X-rays were generated with an exposure factor of 120kV and 100 mA using a standard spiral scan routine. Beam hardening artefacts were minimized using an aluminium filter. Images were collected at 0.8 mm slice intervals. The resolution of the scanners output device was 512 x 512 and the final spatial resolution of each volume unit (voxel) was 0.07 mm^3 ($x = 0.5 \text{ mm}$, $y = 0.5 \text{ mm}$, $z = 0.8 \text{ mm}$). Each scan took less than 10 seconds and, after reconstruction (approximately 30 minutes per scan), generated approximately 150 images. Using public domain software ImageJ 1.21 (National Institutes of Health, USA), an image processing routine was developed to segment the reconstructed grayscale images (in Hounsfield Units, a measure of material density/attenuation value) into binary images of soil pore space that involved the use of Fourier Transform filters. The pore size distributions and the positions of their centres in the image were extracted to data files.

Model development

The pore network based on the soil structural images consists of the vertices corresponding to the centres of the pores and the edges connecting the vertices. The measure for pore connectivity follows the complex network theory (Latora et al., 2001; Cruciti et al., 2003).

The efficiency of the connection between the vertices i and j is defined as:

$$\varepsilon_{ij} = 1/d_{ij} \quad (1)$$

where d_{ij} is the distance between the two vertices. To introduce the influence of the area of the individual pore we set the following measure for the connectivity between the two pores with areas S_i and S_j at the (Euclidian) distance r_{ij} apart:

$$c_{ij} \propto \frac{S_i S_j}{r_{ij}^m} \quad (2)$$

Introducing the parameter m enabled the construction of networks with different properties as described below. If we view the (normalized for the specific network) connectivity defined above as a probability for the two pores to be connected then according to eq. (2) this probability will generally be high for larger pores close together and low for distant smaller pores. Choosing the cut-off value for the connectivity, c_{min} , we can follow the build-up of the pore network with increasing pores being connected (those for which $c_{ij} > c_{min}$) as we lower the cut-off value. Figure 1 shows a typically binary soil structural image and the small pore network constructed applying eq. (2) for connectivity with a high cut-off value so only a few pores are connected. In figure 2, the construction of the soil pore network as the cut-off value for the connectivity is decreased as shown where the emergence of a few highly connected

vertices can be observed. This feature is typical for the scale-free networks (Albert and Barabasi, 2002) which in general show a power-law degree distribution:

$$P(k) \propto k^{-\gamma} \quad (3)$$

where $P(k)$ is the probability that the random chosen vertex will have k edges or links to other vertices. We calculated the degree distributions for two large networks constructed from the binary image using different exponents' m in eq. (2) for connectivity (Figure 3). The degree distributions are fairly well described with the power-law function, the exponent γ depending on the chosen m value. Using the definitions of global and local efficiencies of networks (Latora and Marchiori, 2001; Cruciti et al., 2003) we measured the clustering and the average distance. Small-world networks exhibit both high local and global efficiency (>0.1) while scale-free networks usually exhibit high local and lower global efficiency although scale-free networks with high clustering have also been constructed (Cruciti et al., 2003). The global efficiency is defined as the average efficiency between two vertices in the network of N nodes:

$$E(G) = \frac{1}{N(N-1)} \sum_{i \neq j \in G} \varepsilon_{ij} \quad (4)$$

Since E is defined also for the disconnected graph, the local efficiency E_{loc} is also a useful measure and defined as average efficiency of local subgraphs G_i (consisting of vertices connected to vertex i) of each vertex:

$$E_{loc} = \frac{1}{N} \sum_{i \in G} E(G_i) \quad (5)$$

We calculated the dependence of local and global efficiency of the pore network on the value of the exponent in the definition of connectivity (eq. (3)) (Figure 4).

Random walk simulation and correlations

The transport properties of porous systems often show anomalous behaviour such as non-Fickian diffusion previously observed in soils (e.g. Crawford et al., 1993; Horgan and Ball, 1994). Gallos (2004) demonstrated sub-diffusive behaviour also on scale-free networks. Such dynamics can be characterised by the sub-linear time dependence of mean square displacement of a random walker:

$$\langle \Delta r^2(t) \rangle \propto t^p \quad (6)$$

where $p < 1$. We performed random walk simulations on the images of soil structure such as in figure 1 to try to detect the nature of transport properties. In the numerical experiment, the random walker started from the pore nearest the centre of the image and randomly choose the direction and the size of the step (up to a maximum length set to prevent trapping at a single pore) to perform the walk which was executed if the step ended at another pore point. Figure 5 shows one of the realizations of the random walk on the 2-D soil structure image and the time dependence of the mean square distance averaged over many simulated walks. The sub-diffusive behaviour was observed with the value of the exponent in eq. (6) $p=0.75$. The same numerical experiment was performed also on the randomly generated image with the same porosity. This time normal diffusion was observed as expected.

Some of the morphological information from 2-D soil images can be revealed by computing the correlation functions, useful also in 3-D reconstruction from 2-D images (Yeong and Torquato, 1998a). The normalized two-point correlation function is written as:

$$g(\vec{r} - \vec{r}_0) = \frac{\langle h(\vec{r}_0)h(\vec{r}) \rangle - \phi^2}{\phi(1 - \phi)} \quad (7)$$

where the function h is defined with:

$$h(\vec{r}) = \begin{cases} 1, & \text{if } \vec{r} \text{ at pore} \\ 0, & \text{otherwise} \end{cases} \quad (8)$$

and $\phi = \langle h(\vec{r}_0)h(\vec{r}_0) \rangle$ is the porosity. For an isotropic media, the correlation function depends only on the distance $g(r)$. The computed correlation function (averaged over two perpendicular directions) for an example 2-D soil structure image is shown in figure 6. The correlation function for the random image with the same porosity as an actual 2-D soil section was computed. The correlation function of the soil image can be described with the power-law expression:

$$g(r) = \left(\frac{r + r_0}{r_0} \right)^{-s} \quad (9)$$

while the randomly generated image can best be described with the stretched exponential expression:

$$g(r) = \exp\left(-\left(r/r_0\right)^s\right) \quad (10)$$

The soil pore structure exhibited larger correlations values for short distances compared to the random image and slower decay of correlations than the two phase Debye random media (Yeong and Torquato, 1998b) in which one phase consists of random shapes and sizes. The analysis of the soil images and the constructed complex network illustrates it is possible to view the soil pore architecture as a complex network with, probably, scale-free characteristics.

Model validation

Here we introduce an algorithm to compute a binary image that statistically resembles the soil images, but is built on the underlying scale-free network. The start point is two randomly chosen vertices in an empty array that are connected. New vertices are then added in successive steps. Considering the network of M vertices is already constructed. In the next step a new vertex at a randomly chosen site $a=(i,j)$ is introduced. The vertex to which the new one is to be connected is chosen randomly out of the set of already existing M . The new vertex is added to the network with the probability depending on the degree of the chosen existing vertex (i.e. the number of links) p_b at site $b=(k,l)$ and the distance between the chosen existing and the new vertex: $\propto p_b / r_{ba}$. The new vertices are therefore preferentially attached to close sites with high connectivity. Figure 7 presents the construction of the 2-D image with the underlying complex network. The computation is completed when the desired porosity is reached. Figure 8 shows the computed correlation functions for the simulated and actual 2-D soil image. We observed close matching of the correlation properties between the simulated and actual image which both can be well described by eq. (9). For comparison, the correlation function of the random image with the same size and porosity is added. Finally, we computed a 3-D image based on the complex network construction described above. The resulting

image is presented in figure 9 along with the 3-D soil pore space reconstructed from the stack of 2-D X-ray CT soil scans. We observed that the computed 3-D pore space architecture based on the underlying scale-free network closely resembles the 3-D reconstructed pore space even though it was computed without any pore specific reference to the real soil sample besides the volume of the sample and the porosity.

Conclusions

We have presented the construction of the soil porous architecture model based on the analysis of the 2-D X-ray CT soil scans. Our model of the soil porous architecture is built on the complex network with scale-free degree distribution. The computed binary images based on underlying pore complex network showed a close match of the correlation properties with the experimentally obtained image giving a good link with the model derived porous structures. These results are a positive indication that the porous networks in soils, albeit only for one soil type, have indeed scale-free properties. This is likely to have important consequences for the further investigations and understanding of structure and transport properties of soils.

References

- Albert, R. and Barabasi, A. -L. 2002. Statistical mechanics of complex networks. *Rev. Mod. Phys.* **74**, 47–97.
- Bird, N., Cruz Diaz, M., Saab A., and Tarquisc, A.N. 2006. Fractal and multifractal analysis of pore-scale images of soil. *J. Hydrol.*, **322**, 211–219.

Blair, J.M., Falconer, R.E., Milne, A.C., Young, I.M. and Crawford, J.C. 2007. Modeling Three-dimensional microstructure in heterogenous media. *Soil. Sci. Soc. Am. J.*, **71**, 1807-1812.

Cislerova, N. 1999. Characterization of pore geometry. In: Proceedings of the International Workshop on modelling of transport processes in soils at various scales in time and space. Leuven, Belgium.

Crawford, J.W., Ritz, K. and Young, I.M. 1993. Quantification of fungal morphology, gaseous transport and microbial dynamics in soils: an integrated framework utilising fractal geometry. *Geoder.*, **56**, 157-172.

Cruciti, P., Latora, V., Marchiori, M. and Rapisarda, A. 2003. Efficiency of Scale-Free Networks: Error and Attack Tolerance. *Physica A*, **320**, 642.

Gallos, L.K. 2004. Random walk and trapping processes on scale-free networks. *Physical Reviews E*, **70**, 46-116.

Horgan, G.W. and Ball, B.C. 1994. Simulating diffusion in a Boolean model of soil pores. *Eur. J. Soil Sci.*, **45**, 483-491.

Kim, B.J., Trusina, A., Minnhagen, P. and Sneppen, K. 2005. Self Organized Scale-Free Networks from Merging and Regeneration. *Eur. Phys. J. B*, **43**, 369-372.

Latora, V. and Marchiori, M. 2001. Efficient behavior of small-world networks. *Phys. Rev. Lett.*, **87**, 11–14.

Lin, H.S., McInnes, K.J., Wilding, L.P., and Hallmark, C.T. 1999. Effects of Soil Morphology on Hydraulic Properties. I. Quantification of Soil Morphology. *Soil Sci. Soc. Am. J.* 63:948-954

Newman, M.E.J. 2003. The structure and function of complex networks. *SIAM Rev.*, **45**, 167–256.

Prosperini, N., D. Perugini, D. 2007. Application of a cellular automata model to the study of soil particle size distributions. *Physica A*, **388**, 595-602.

Song, C., Havlin, S. and Makse, H.A. 2005. Self-similarity of complex networks. *Nature*, **433**, 392-395.

Spanne, P., Thovert, J.F., Jacquin, C.J., Lindquist, W.B., Jones, K.W. and Adler, P.M. 1994. Synchrotron computed microtomography of porous media: topology and transports. *Phys. Rev. Lett.*, **73**, 2001-2004.

Valentini, L., Perugini, D. and Poli, G. 2007. The “small-world” topology of rock fracture networks. *Physica A*, **377**, 323-328.

Vogel, H.-J. 1997. Morphological determination of pore connectivity as a function of pore size using serial sections. *Eur. J. Soil Sci.*, **48**, 365-377.

Vogel, H.-J. and Roth, K. 2001. Quantitative morphology and network representation of soil pore structure. *Advances in Water Resources*, **24**, 233-242.

Vogel, H.-J., Tölke, J., Schulz, V. P., Krafczyk, M., and Roth, K. 2005: Comparison of a Lattice-Boltzmann model, a full-morphology model, and a pore network model for determining capillary pressure-saturation relationships, *Vadose Zone J.*, **4**, 380-388.

Yeong, C.L.Y. and Torquato, S. 1998a. Reconstructing random media. *Phys. Rev. E*, **57**, 495-506.

Yeong, C.L.Y. and Torquato, S. 1998b. Reconstructing random media. II. Three-dimensional media from two-dimensional cuts. *Phys. Rev. E*, **58**, 224-233.

Young, I.M. and Crawford, J.W. 2004. Interactions and Self-Organization in the Soil-Microbe Complex. *Science*, **304**, 1634-1637.

List of Figures

Figure 1: 2D X-CT binary image of undisturbed soil sample. Pores are shown as black areas. Superimposed on the soil image is the constructed network at high cut-off value (i.e. small number of edges) for the pore connectivity (eq. (2)) with $m=1$.

Figure 2: Network of the soil pore architecture with decreasing cut-off (i.e. increasing number of vertices and edges) of pore connectivity from top left to bottom right. The positions of the vertices correspond to the pore areas in the image shown in fig.1.

Figure 3: Examples of pore networks architecture constructed from the image shown in fig.1 with their degree distributions in log-log scale. Networks presented here are in an abstract way, the vertices do not correspond to the actual positions of the pores in the image as in fig.2. The upper network was constructed with the exponent of the connectivity $m=5$, and with the cut-off value set to results in the network with 2000 edges. The connectivity exponent for the lower network was $m=3$, and the network has 1000 edges. The exponent of the power-laws plotted in degree distributions are $\gamma = 2,3$ (upper) and $\gamma = 1,4$ (lower). The calculated global and local efficiencies for the two networks shown here are: $E_{glob} = 0,16$ and $E_{loc} = 0,41$ for the upper, and $E_{glob} = 0,25$, $E_{loc} = 0,20$ for the lower network.

Figure 4: Dependence of local (triangles) and global (dots) efficiency of the pore network on the value of the exponent in the definition of connectivity (eq. (2)). Left: networks constructed with constant number of edges (=2000). Right: networks constructed with constant number of vertices (=400).

Figure 5: Left: normalized mean squared distance as a function of steps (time) of the computed random walk on pores in soil image of fig.1. The solid lines are plots of eq. (6) with the exponents $p = 1.0$ and $p = 0,75$ for the upper and lower data sets respectively. The data sets on the left figure are the averaged over a large number of random walks. Lower data set represent the results for the random walk where the allowed jumps always end on a pore (black area in the soil image), while the upper data set shows the results of the random walk on the random image with the same porosity as the actual one. Right: single realization of the random walk superimposed on the actual 2D soil image.

Figure 6: Two-point normalized correlation function of the soil pore structure computed from the soil image in fig.1 (open dots) and for the random image with the same porosity. The solid lines are plots of eqs. (9) and (10) with $r_0 = 27$, $s=2,2$ for the soil image, and $r_0=4$, $s=0,4$ for the random image.

Figure 7: Construction of the 2D binary image of pore architecture (left panel) based on complex network model with preferential attachment rule for pore connectivity. Left panel shows the progressive build-up of the image as new pores are introduced to the image. The simulation is stopped when the desired porosity is achieved. Image on the right is the actual 2-D X-ray CT scan of the soil sample.

Figure 8: Normalized two-point correlation function for the simulated soil image (stars), the actual X-ray CT scan (open dots), and for the random image with the same porosity. The full lines are the plots of the correlation functions according to eq. (9) and (10) with

$r_0 = 4, s=2,3$ for the soil and for the simulated soil image, and $r_0=1, s=0,65$ for the random image.

Figure 9: Left: 3D reconstruction of the soil pore architecture from stack of X-ray CT scans. The pore space is shown while the soil matrix is here transparent. Right: 3D model of the soil pore architecture based on the pore complex network with preferential attachment rule for the pore connectivity.

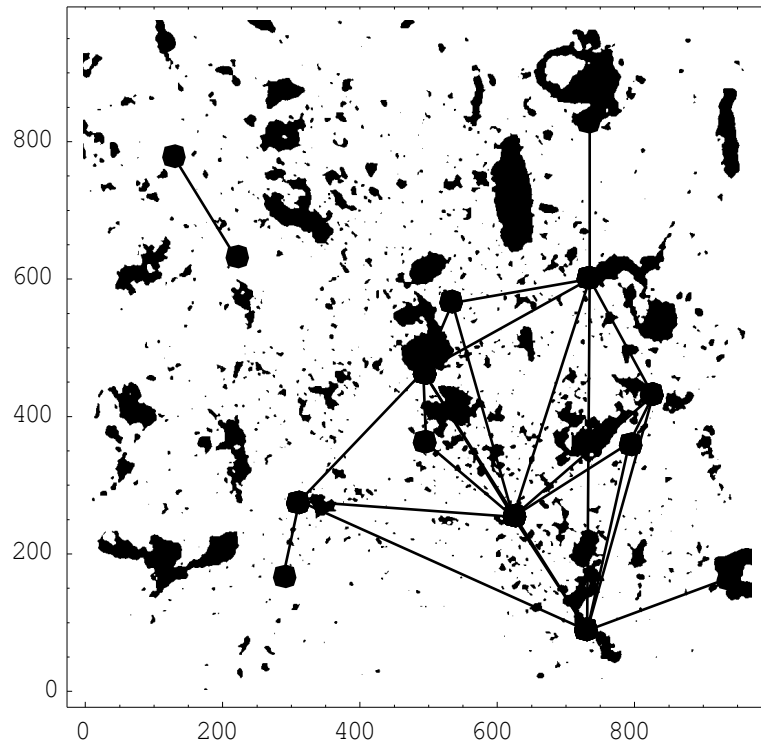


Figure 1: 2D X-CT binary image of undisturbed soil sample. Pores are shown as black areas. Superimposed on the soil image is the constructed network at high cut-off value (i.e. small number of edges) for the pore connectivity (eq. (2)) with $m=1$.

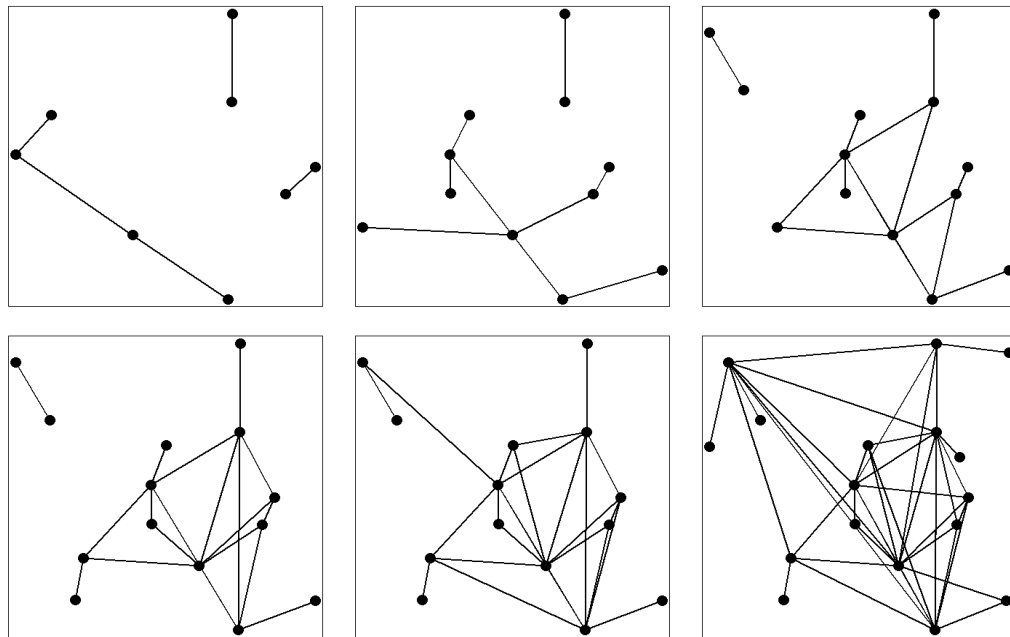


Figure 2: Network of the soil pore architecture with decreasing cut-off (i.e. increasing number of vertices and edges) of pore connectivity from top left to bottom right. The positions of the vertices correspond to the pore areas in the image shown in fig.1.

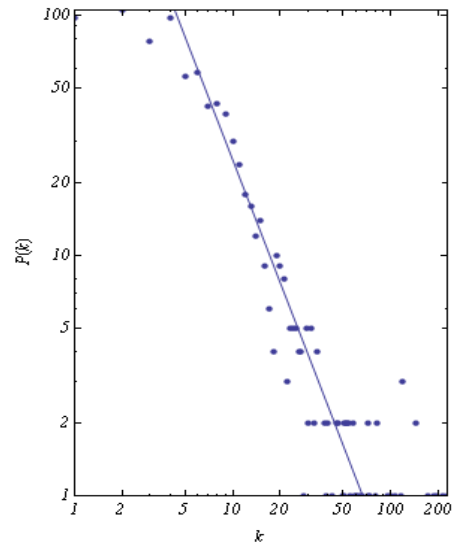
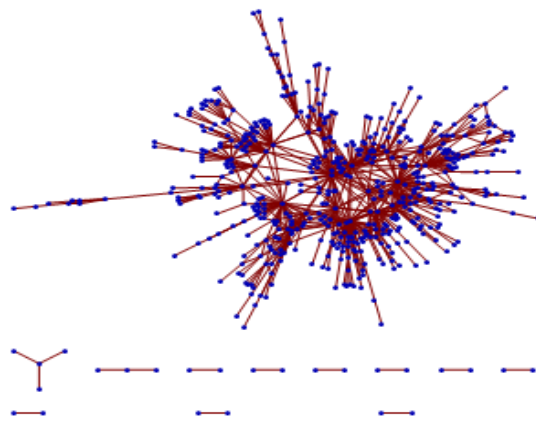
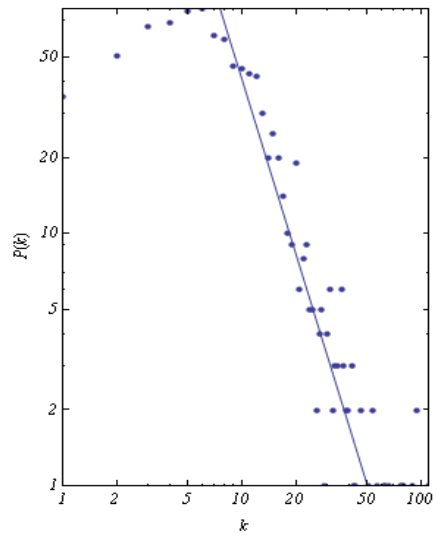
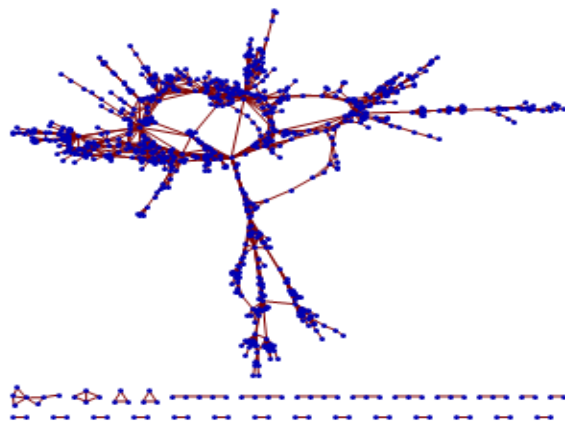


Figure 3: Examples of pore networks architecture constructed from the image shown in fig.1 with their degree distributions in log-log scale. Networks presented here are in an abstract way, the vertices do not correspond to the actual positions of the pores in the image as in fig.2. The upper network was constructed with the exponent of the connectivity $m=5$, and with the cut-off value set to results in the network with 2000 edges. The connectivity exponent for the lower network was $m=3$, and the network has 1000 edges. The exponent of the power-laws plotted in degree distributions are $\gamma = 2,3$ (upper) and $\gamma = 1,4$ (lower). The calculated global and local efficiencies for the two networks shown here are: $E_{glob} = 0,16$ and $E_{loc} = 0,41$ for the upper, and $E_{glob} = 0,25$, $E_{loc} = 0,20$ for the lower network.

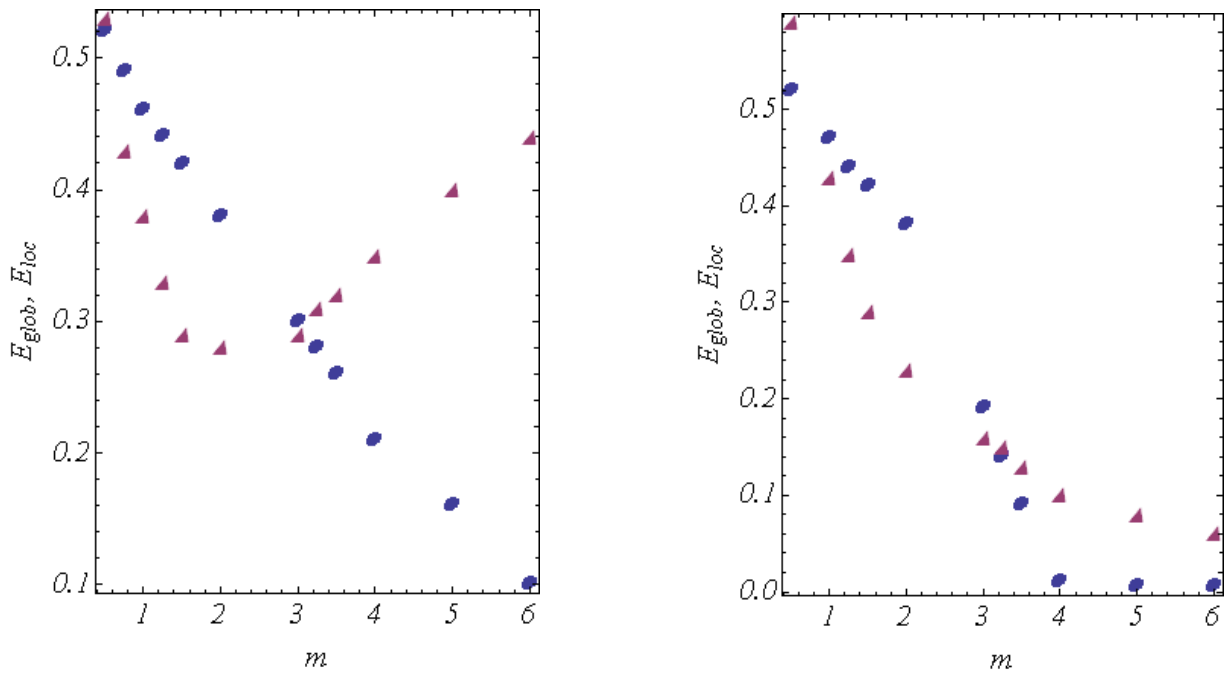


Figure 4: Dependence of local (triangles) and global (dots) efficiency of the pore network on the value of the exponent in the definition of connectivity (eq. (2)). Left: networks constructed with constant number of edges (=2000). Right: networks constructed with constant number of vertices (=400).

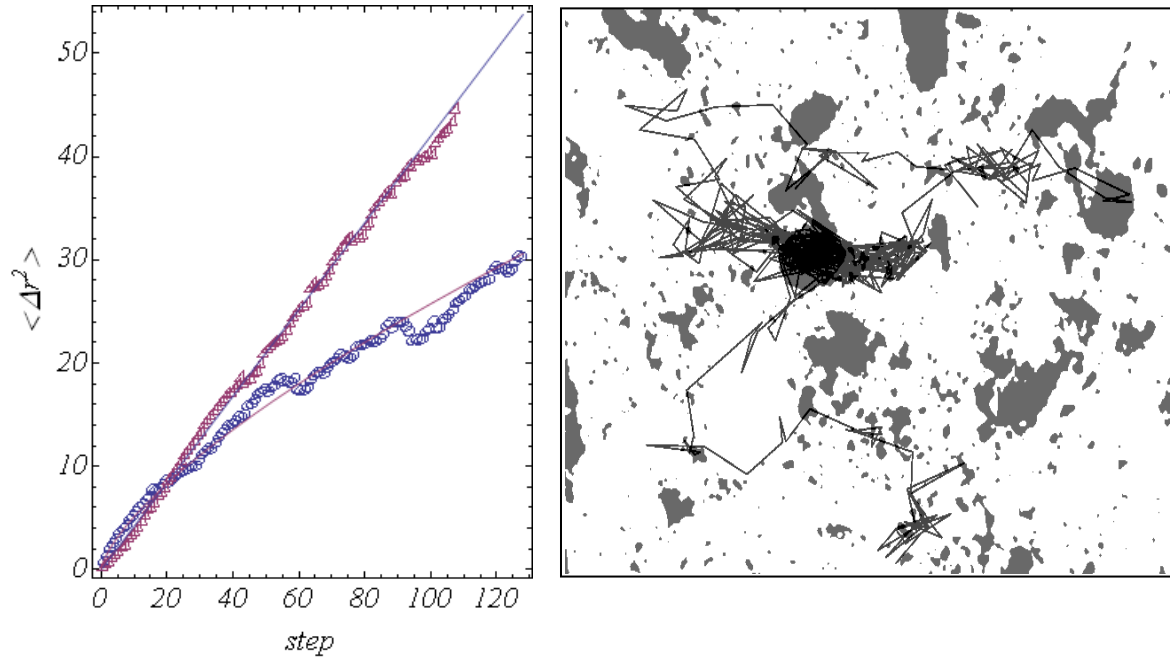


Figure 5: Left: normalized mean squared distance as a function of steps (time) of the computed random walk on pores in soil image of fig.1. The solid lines are plots of eq. (6) with the exponents $p = 1.0$ and $p = 0,75$ for the upper and lower data sets respectively. The data sets on the left figure are the averaged over a large number of random walks. Lower data set represent the results for the random walk where the allowed jumps always end on a pore (black area in the soil image), while the upper data set shows the results of the random walk on the random image with the same porosity as the actual one. Right: single realization of the random walk superimposed on the actual 2D soil image.

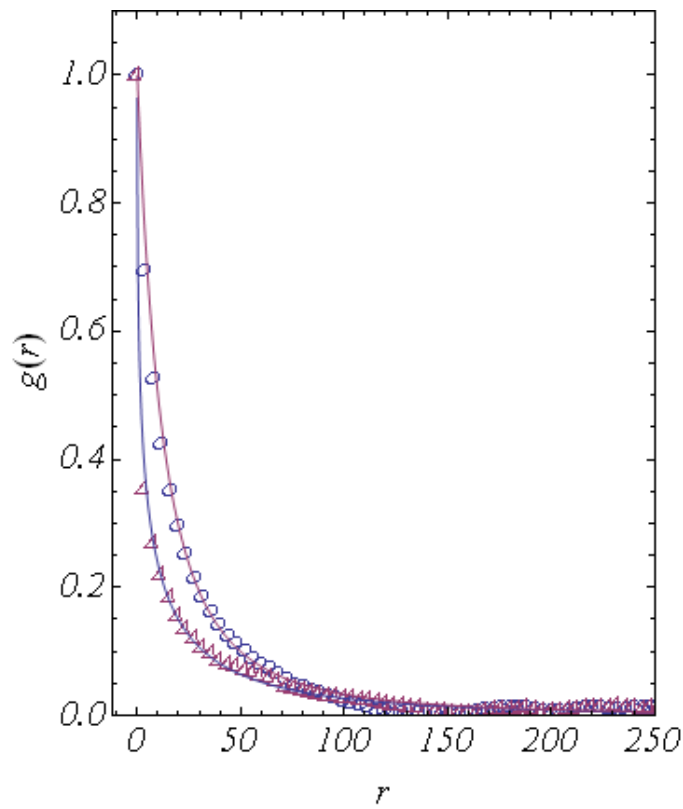


Figure 6: Two-point normalized correlation function of the soil pore structure computed from the soil image in fig.1 (open dots) and for the random image with the same porosity. The solid lines are plots of eqs. (9) and (10) with $r_0 = 27$, $s = 2,2$ for the soil image, and $r_0 = 4$, $s = 0,4$ for the random image.

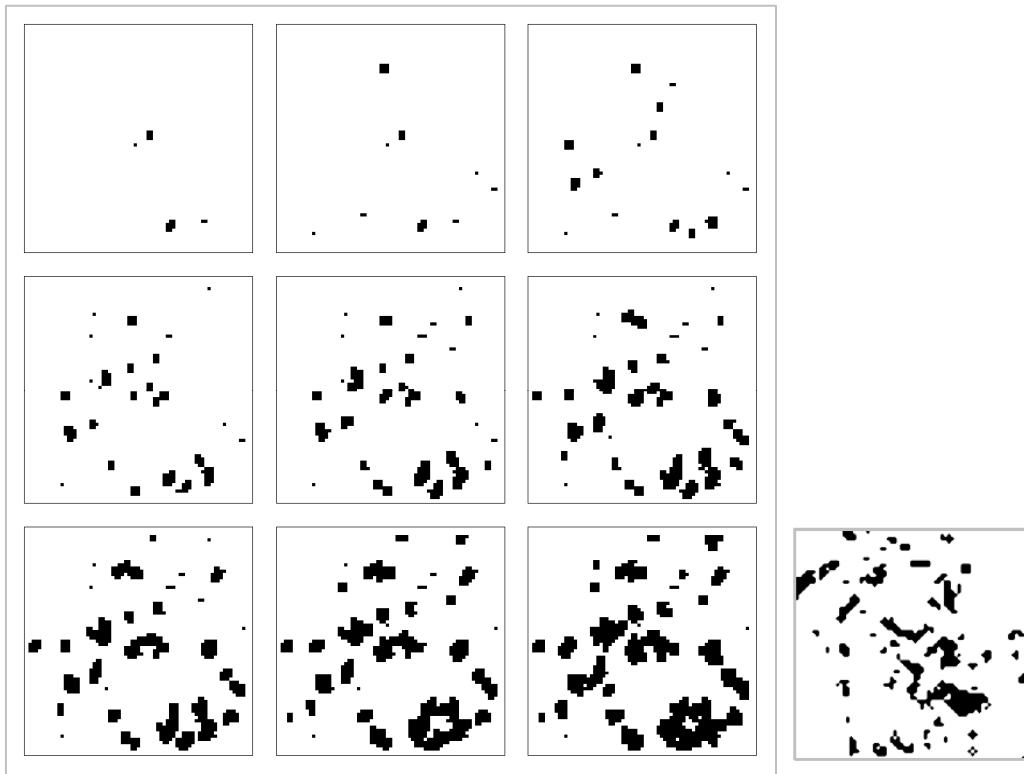


Figure 7: Construction of the 2-D binary image of pore architecture (left panel) based on complex network model with preferential attachment rule for pore connectivity. Left panel shows the progressive build-up of the image as new pores are introduced to the image. The simulation is stopped when the desired porosity is achieved. Image on the right is the actual 2-D X-ray CT scan of the soil sample.

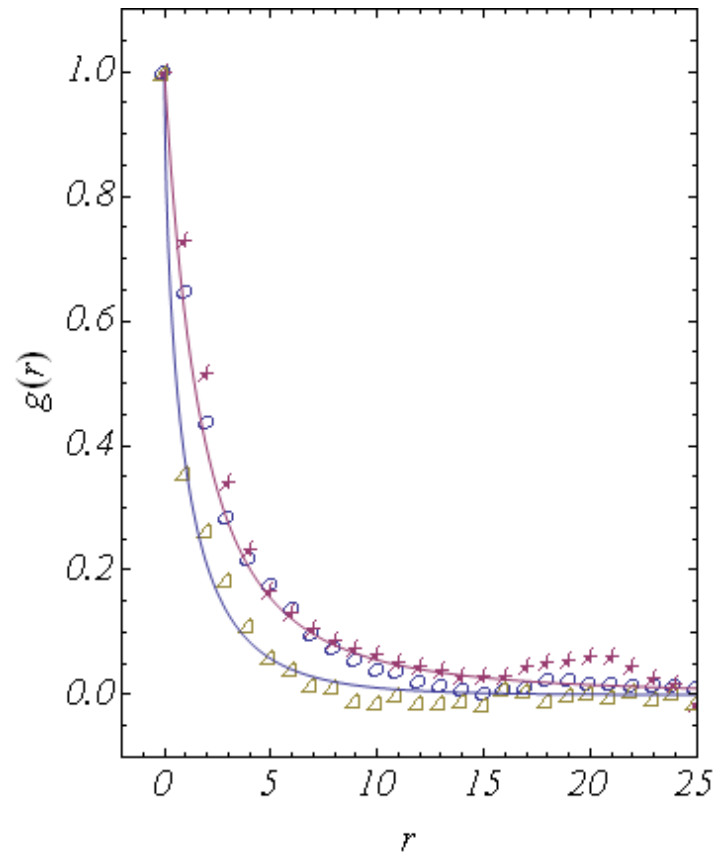


Figure 8: Normalized two-point correlation function for the simulated soil image (stars), the actual X-ray CT scan (open dots) and for the random image with the same porosity. The full lines are the plots of the correlation functions according to eq. (9) and (10) with $r_0 = 4$, $s=2,3$ for the soil and for the simulated soil image, and $r_0=1$, $s=0,65$ for the random image.

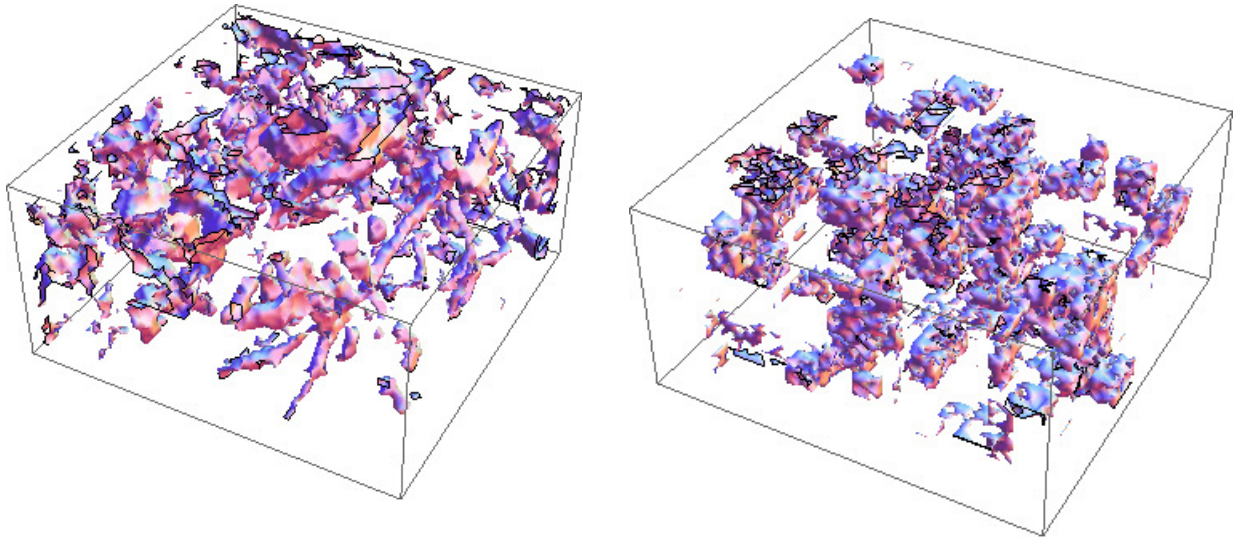


Figure 9: Left: 3-D reconstruction of the soil pore architecture from stack of X-ray CT scans. The pore space is shown while the soil matrix is here transparent. Right: 3-D model of the soil pore architecture based on the pore complex network with preferential attachment rule for the pore connectivity.